Vol. 15, No. 1, 2024
ISSN 2233-4203/ e-ISSN 2093-8950
REVIEW www.msletters.org | Mass Spectrometry Letters

Gold Nanostructure-Based Laser Desorption/Ionization Time-of-Flight Mass Spectrometry for Analysis of Small Biomolecules

Hye-Sun Cho[1], Tae Hoon Seo[2]*, Ji Hun Park[3]*, and Young-Kwan Kim[1]*

[1]*Department of Chemistry, Dongguk University-Seoul, Seoul 04620, Republic of Korea*
[2]*Energy & Nano Technology Group, Korea Institute of Industrial Technology, Gwangju 61012, Republic of Korea*
[3]*Department of Science Education, Ewha Womans University, Seoul 03760, Republic of Korea*

Received March 19, 2024; Revised March 26, 2024; Accepted March 26, 2024
First published on the web March 31, 2024; DOI: 10.5478/MSL.2024.15.1.26

Abstract : Gold nanostructures (Au NSs) are useful and interesting matrices for mass spectrometric analysis of various biomolecules based on organic matrix-free laser desorption/ionization time-of-flight mass spectrometry (LDI-TOF-MS). Au NSs provide high efficiency and versatility in LDI-TOF-MS analysis based on their well-established synthesis and surface functionalization, large surface area, high laser absorption capacity, and photothermal conversion efficiency. Therefore, Au NSs based LDI-TOF-MS can be a facile, functional, and efficient analytical method for important small biomolecules owing to its simple preparation, rapid analysis, salt-tolerance, signal reproducibility, and quantitative analysis. This review chronologically summarizes the important advance of Au NSs-based LDI-TOF-MS platforms in terms of in-depth mechanism, signal enhancement, quantitative analysis, and disease diagnosis.

Keywords : gold nanostructure, nanohybrid, laser, mass spectrometry, small molecules

Introduction

Since the pioneering work of Karas et al., matrix-assisted laser desorption/ionization time-of-flight mass spectrometry (MALDI-TOF-MS) has been considered one of the most important analytical techniques to analyze an intact molecular weight of large molecules such as proteins, nucleic acids, and synthetic polymers without fragmentation (Figure 1).[1] This analytical technique has significantly contributed to advances in proteomics, biology, and pharmacology based on its simplicity, high resolution, and sensitivity.[2] Therefore, there has been a strong demand to utilize MALDI-TOF-MS for mass spectrometric analysis of various small molecules (< 500 Da), but MALDI-TOF-MS cannot be directly applied to analysis of low molecular weight compounds owing to drawbacks derived from conventional organic matrices such as matrix interference in low mass region, heterogeneous co-crystallization, and sublimation under a high vacuum.[3] Especially, the matrix interference originates from the photochemical reactions of organic matrices by laser irradiation during MALDI-TOF-MS analysis and complicates the obtained mass spectra.[4]

To avoid the matrix interference, many efforts have been devoted to development of an efficient analytical platform for organic matrix-free laser desorption/ionization time-of-flight mass spectrometry (LDI-TOF-MS).[5] Although Tanaka et al. reported in 1988 that cobalt nanoparticles (NPs) dispersed in glycerol can desorb and ionize proteins and synthetic polymers for mass spectrometric analysis,[6] nanostructures (NSs) have been not widely harnessed for LDI-TOF-MS owing to the introduction of organic matrices. In the early studies, the major applications of LDI-TOF-MS are mass spectrometric analysis of large molecules, and thus there was no strong motivation to utilize NSs for LDI-TOF-MS analysis. After Siuzdak et al. demonstrated an efficient desorption/ionization on porous silicon (DIOS) for mass spectrometric analysis of small molecules,[7] various NSs having unique physicochemical properties have been extensively investigated to find an optimal analytical platform.[8] The widely explored NSs can

Open Access
*Reprint requests to Tae Hoon Seo
https://orcid.org/0000-0002-9896-6404
E-mail: thseo@kitech.re.kr
*Reprint requests to Ji Hun Park
https://orcid.org/0000-0001-8218-0823
E-mail: jihunpark@ewha.ac.kr
*Reprint requests to Young-Kwan Kim
https://orcid.org/0000-0002-9929-9510
E-mail: kimyk@dongguk.edu

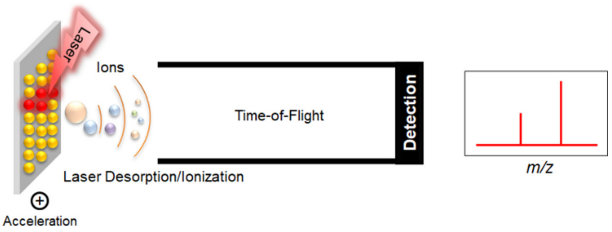

Figure 1. Schematic diagram of LDI-TOF-MS on the Au NSs for analysis of various small molecules.

be categorized into porous silicons,[9] carbonized metal-organic-frameworks (MOF),[10] transition metal dichalcogenides,[11] quantum dots,[12] MXene,[13] metal,[14] and carbon nanomaterials.[15]

Among the various NSs, Au NSs are of particular importance owing to their well-established synthesis and surface functionalization, low specific heat capacity, high stability, laser energy absorption capacity, and photothermal conversion efficiency (Figure 1).[16] The laser desorption/ionization (LDI) process on Au NSs is also elucidated with systematic studies using a model thermometer molecule.[17] When Au NSs are irradiated with a pulsed laser, electrons in Au NSs interact with the incident laser, and they are excited to a higher energy level. Those electrons at the high energy state, hot electrons, are relaxed to the ground state with releasing a significant thermal energy to surroundings.[17] During this photothermal conversion process on Au NSs, LDI of small molecules is generally driven by two representative mechanisms such as photothermal desorption and photothermal phase transition.[17] The photothermal desorption mechanism leads to LDI through the direct thermal energy transfer from Au NSs to small molecules whereas the photothermal phase transition mechanism results in LDI through the non-thermal desorption process by photothermal restructuring/melting of Au NSs.[17]

The efficiency of Au NSs in LDI-TOF-MS analysis can be considerably enhanced by the designed synthesis with various morphologies,[18] appropriate suface functionalization,[19] surface immobilization with a high coverage,[20] and ordered self-assembly on a substrate.[21] In addition to the problematic issues of organic matrices, those Au NSs provide many advantages for LDI-TOF-MS analysis such as high salt tolerance, signal reproducibility, and target specific enrichment which are highly desirable for forensic, pharmaceutical, environmental, and biomedical research fields.[21] In this review, we mainly discuss the strategies to improve sensitivity, signal reproducibility, and applicability of Au NSs as a matix for the efficient and functional LDI-TOF-MS analysis of various small molecules. In addition, the perspectives and remaining challenges are also provided for future development of the practical Au NS-based LDI-TOF-MS platform.

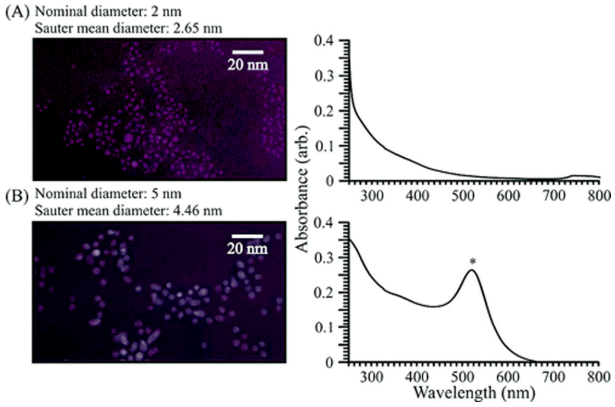

Figure 2. Transmission electron microscopy (TEM) images and UV-visible absorption spectra of 2 nm and 5 nm Au NPs. The asterisk indicated LSPR band of 5 nm Au NPs. Reprinted with permission from McLean et al. (2005). Copyright 2005 American Chemical Society.

Synthesis of Au nanoparticles (NPs) with different morphology for LDI-TOF-MS analysis

The spherical Au NPs have been extensively studied for LDI-TOF-MS analysis owing to their easy synthesis and facile surface functionalization.[22] The primary role of Au NPs lies in the concentration of samples through selective adsorption of analytes and subsequent photothemral conversion for LDI-TOF-MS analysis.[16] To effectively perform these two roles, Au NPs are required to have a high surface area, porosity, facile surface functionalization, high optical absorption, and thermal conductivity.[16] Russell et al. demonstrated LDI-TOF-MS efficiency of Au NPs is highly dependent on their size by using 2, 5, and 10 nm sized Au NPs (Figure 2).[23] 2 nm-sized Au NPs exhibited a much higher LDI efficiency than 5 and 10 nm sized Au NPs. This size-dependent LDI efficiency of Au NPs was attributed to the quantum confinement effect which leads to electronic excitation and subsequent energy transfer for ionization of analytes. Specifically, the mass signal intensity of a peptide (1,347.64 Da) increased with decreasing size of Au NPs (Figure 3).[23]

After this finding, Au NPs are extensively investigated as a matrix for LDI-TOF-MS analysis,[16] and thus various synthetic strategies are harnessed for the synthesis of Au NPs with different morphologies to explore the morphological effect on LDI-TOF-MS analysis. Since Au NPs have a high applicability for optical, electronic, and biomedical research fields, the synthetic strategies have been well established for size- and shape-controlled synthesis of Au NPs.[22] It is well-known that the optical absorption properties of Au NPs depend on their size and shape.[22] Russell et al. utilized Au nanorods (Au NRs) functionalized with 4-aminothiophenol (4-ATP) as a matrix for LDI-TOF-MS analysis (Figure 4).[24] In this case, IR laser was used to induce the localized surface plasmon resonance (LSPR) on Au NRs along with their longi-

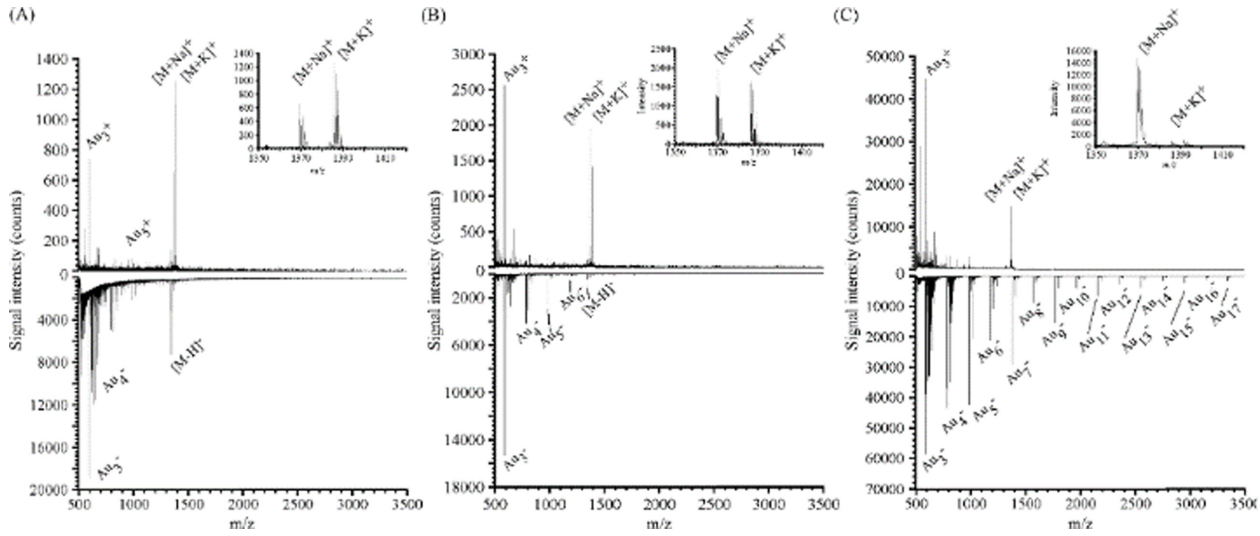

Figure 3. LDI-TOF-MS spectra of a peptide (RPKPQQFFGLM-NH_2, 1,347.64 Da) obtained with (a) 2 nm, (b) 5 nm, and (c) 10 nm Au NPs. McLean et al. (2005). Copyright 2005 American Chemical Society.

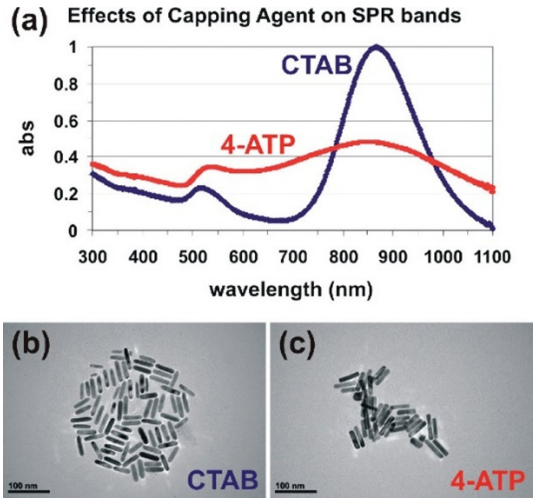

Figure 4. (a) UV-visible absorption spectra of Au NRs and 4-ATP-Au NRs. (b) TEM images of Au NRs and (c) 4-ATP-Au NRs. Reprinted with permission from Castellana et al. (2010). Copyright 2010 American Chemical Society.

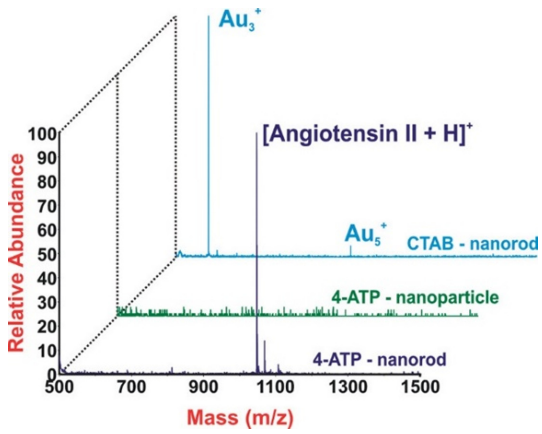

Figure 5. LDI-TOF-MS spectra of angiotensin II (1,045.5 Da) obtained by using IR laser (1,064 nm) with 4-ATP-Au NRs (dark blue line), 4-ATP-Au NPs (green line), and as synthesized Au NRs (light blue line). Reprinted with permission from Castellana et al. (2010). Copyright 2010 American Chemical Society.

tudinal axis, and the 4-ATP functionalized Au NRs lead an efficient LDI-TOF-MS analysis of an angiotensin II (1,045.5 Da) (Figure 5).[24]

Martínez–Haya et al. synthesized Au nanosphere, Au nanostar, and Au NRs. LDI efficiency of the synthesized Au NSs was systematically compared for LDI-TOF-MS analysis of polyethylene glycol (PEG, 600 Da).[18] The LSPR bands of Au nanosphere, Au nanostar, and Au NRs are varied depending on their morphology, and thus their light-matter interaction with laser equipped in LDI-TOF-MS is different based on the excitation wavelengths (266, 355, 532, and 1,064 nm). The LDI-TOF-MS spectra of PEG obtained with all tested conditions confirmed that the LDI efficiency of Au NPs was higher at 532 nm corresponding to their LSPR bands than 355 nm which is conventional wavelength of UV laser equipped in LDI-TOF-MS. Those results showed that the shape controlled synthesis and appropriate selection of laser wavelength are significant for successful LDI-TOF-MS analysis.

Surface functionalization of Au NPs for efficient LDI-TOF-MS analysis

The surface functionalization of Au NPs with thiol ligands has been extensively investigated to enhance their

biocompatibility, biological functions, and colloidal stability.[25] The surface of Au NPs is spontaneously modified with various thiol ligands through Au-S interaction.[26] The resulting molecular layer of thiol ligands is well-ordered with a compacted structure, and thus it is called self-assembled monolayers (SAMs).[26] The surface functionalization is also important considering that as-synthesized colloidal Au NPs are generally stabilized with an excess amount of trisodium citrate.[27] Therefore, there is abundant alkali metal ions such as Na^+ and K^+ in the colloidal suspension of Au NPs. Those alkali metal ions can be regarded as impurities during LDI-TOF-MS analysis, and thus make LDI-TOF-MS spectrum of small molecules complicated with formation of abundant alkali metal adducts such as $[M + Na]^+$ and $[M + K]^+$ instead of protonated adduct $[M + H]^+$ when colloidal Au NPs are utilized as a matrix for LDI-TOF-MS analysis. For the straightforward analysis of LDI-TOF-MS spectrum, the formation of protonated analyte adducts is highly advantageous compared to the alkali metal adducts.[28] It was previously reported that LDI efficiency of small molecules with the surface functionalized Au NPs was highly enhanced with addition of citric acid as a proton donor.[28] In this regard, the surface functionalization of colloidal Au NPs with thiol ligands can be a simple and efficient strategy to introduce proton donors on their surfaces because alkanethiol ligands with various end functional groups have been extensively investigated to form SAMs on Au surfaces.[26] Russell et al. reported the surface functionalization of Au NPs with 4-ATP ligand for the first time to enhance their efficiency in LDI-TOF-MS analysis (Figure 6).[29] Their hypothesis was that the surface functionalization of Au NPs with proton donating ligands (4-ATP) would increase the ionization efficiency. The 4-ATP functionalized Au (4-ATP-Au) NPs were synthesized through the spontaneous formation of 4-ATP SAMs on the surface of Au NPs through Au-S interaction. The 4-ATP-Au NPs exhibited the highly increased ionization efficiency, decreased ion fragmentation, and increased working molecular weight range compared to pristine Au NPs.

For instance, ACTH peptide (2,465.20 Da) was analyzed using 4-ATP-Au NPs and citrate-stabilized Au NPs to compare their LDI efficiency. The LDI-TOF-MS spectrum of ACTH peptide showed a great increase (3 orders of magnitude) in the ion intensity of $[M+H]^+$ with 4-ATP-Au NPs compared to citrate-stabilized Au NPs (Figure 7). The enhanced LDI performance of 4-ATP-Au NPs was attributed to the proton transfer from 4-ATP to analytes and efficient LDI process with a low internal energy transfer because SAMs of 4-ATP prevent the undesired formation of Au cluster ions and direct adsorption of analytes on the surface of Au NPs. There was another important finding that the working molecular weight range was also 2.5-fold extended with 4-ATP-Au NPs compared to citrate-stabilized Au NPs. The cytochrome c (~12,400 Da) was detected with 4-ATP-Au NPs as its singly and doubly charged ions, but there was no discernible mass signal with citrate-stabilized Au NPs.

Siuzdak et al. also demonstrated that the functionalization of Au NPs with perfluorinated alkanethiol greatly enhanced LDI efficiency for LDI-TOF-MS imaging of metabolites in animal organ tissues.[30] It was previously reported that the nonadherent property of SAMs composed perfluorinated alkanethiols impedes the selective and irreversible adsorption of analytes on the surface of Au NPs.[31] This feature resulted in the successful LDI-TOF-MS imaging of the comprehensive metabolites such as glucose, hydroxycholesterol, phosphocholine, glucosamine, acetic acid, glucose-phosphate, and acetyl-serine in the animal tissues by using

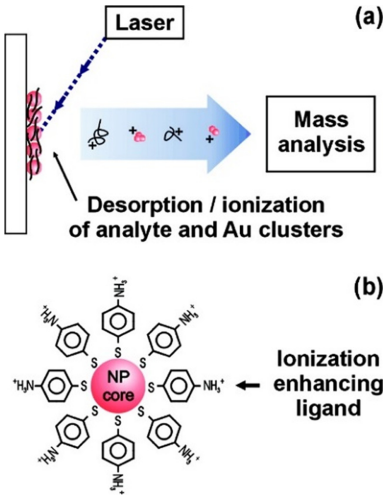

Figure 6. (a) Schematic diagram of LDI-TOF-MS analysis process on Au NPs and (b) 4-ATP-Au NPs. Reprinted with permission from Castellana et al. (2007). Copyright 2007 American Chemical Society.

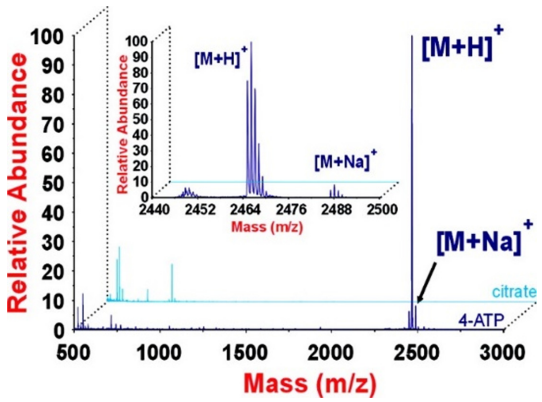

Figure 7. LDI-TOF-MS spectra of a peptide ACTH (18-39) (RPVKVYPNGAEDESAEAFPLEF, 2,465.20 Da) obtained with 4-ATP-Au NPs (dark blue line) and citrate-stabilized Au NPs (light blue line). Reprinted with permission from Castellana et al. (2007). Copyright 2007 American Chemical Society.

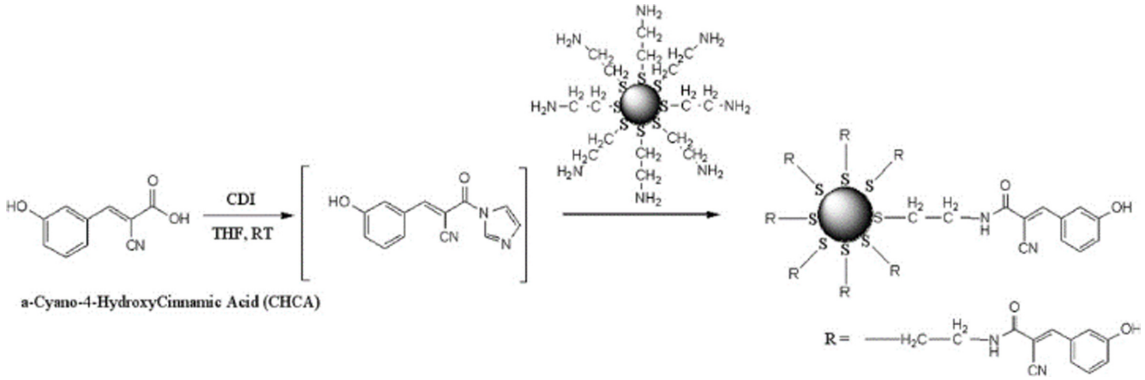

Figure 8. Schematic diagram of the synthetic process of CHCA-Au NPs. Reprinted with permission from Duan et al. (2009). Copyright 2009 American Chemical Society.

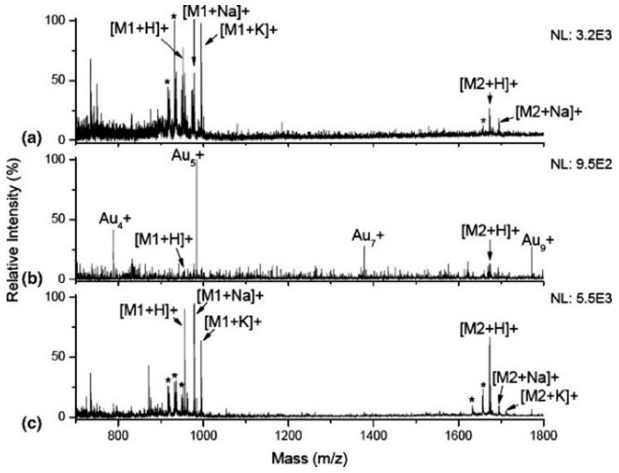

Figure 9. LDI-TOF-MS spectra of peptides such as angiotensin II (M1) and neurotensin (M2) obtained with (a) citrate-stabilized Au NPs, (b) cysteamine-functionalized Au NPs, and (c) CHCA-Au NPs. Mass spectrum of peptides obtained by (a) Au NPs, (b) cysteamine-functionalized Au NPs, and (c) CHCA-Au NPs. Reprinted with permission from Duan et al. (2009). Copyright 2009 American Chemical Society.

perfluorinated Au (F-Au) NPs. The F-Au NPs revealed the significant rearrangement in the metabolic organization of the mouse colon, caused by a fiber and/or polysaccharide depleted diet, based on LDI-TOF-MS imaging process.

The chemistry of SAMs was further employed to immobilize commonly used organic matrix, α-cyano-4-hydroxycinnamic acid (CHCA), on the surface of Au NPs.[28] A sequential process was developed with cysteamine functionalization of Au NPs and subsequent carbonyldiimidazole (CDI) mediated amide coupling reaction for CHCA conjugation on the cysteamine-functionalized Au (Cyst-Au) NPs (Figure 8). The CHCA-functionalized Au (CHCA-Au) NPs showed a highly enhanced LDI efficiency without undesired generation of Au cluster ions compared to as-synthesized and Cyst-Au NPs for LDI-TOF-MS analysis of peptides such as [Sar[1], Thr[8]]-angiotensin II (956.1 Da) and neurotensin (1,672 Da) (Figure 9).[28] The LDI efficiency of CHCA-Au NPs was further enhanced by the addition of glycerol and citric acid as co-additives, and the CHCA-Au NPs maintain their high LDI efficiency for LDI-TOF-MS analysis of peptides even in complex aqueous media.

In addition to the Au-S interactions, polydopamine (pDA) has been also actively explored to functionalize Au NSs for LDI-TOF-MS analysis owing to its high optical absorption, simple and universal coating properties, high biocompatibility, water dispersibility, and facile chemical functionalization.[32] Previously, our group synthesized a pDA coated Au NRs (pDA@Au NRs) through self-oxidative polymerization of dopamine in the presence of Au NRs (Figure 10a).[33] The synthesized pDA@Au NRs exhibited a broad optical absorption UV-Vis region owing to the formation of pDA layer. The LDI behavior of as-synthesized Au NRs and pDA@Au NRs were compared under the equal condition in LDI-TOF-MS analysis. LDI-TOF-MS spectrum of pDA@Au NRs exhibited an only $[CTA]^+$ peak which is a cationic part of the shape directing agent, cetrimonium bromide (CTAB) while there were strong peaks of Au cluster ions in LDI-TOF-MS spectrum of Au NRs (Figure 10b). This result suggest that pDA coating layer suppressed generation of the undesired Au cluster ions during LDI-TOF-MS analysis, and thus there was less laser energy loss through the fragmentation and ionization of Au atoms on the surface of pDA@AuNRs, leading to more efficient LDI with less background noise than Au NRs.

As a result of those effects, the synthetic polymers such as polyethylene glycol (PEG) were successfully analyzed with LDI-TOF-MS by using pDA@Au NRs whereas those were not detected with as-synthesized Au NRs (Figure 10c). This LDI capability was attributed to the high optical absorption and efficient photothermal conversion properties of pDA coating layer. The pDA@Au NRs based LDI-TOF-MS analysis showed a significant potential for synthetic polymers owing to the extended working molecular weight

range. The improvement was ascribed to the versatility of pDA coating layer which avoid undesired generation of Au cluster ions, enhancement of laser energy absorption capacity and photothermal conversion efficiency.

Those important previous reports demonstrated that the surface functionalization of Au NPs can provide a great promise to develop an efficient LDI-TOF-MS platform. However, the detailed enhancement mechanism of LDI process on the surface fuctionalized Au NPs is not clearly understood owing to the complicated system composed of thiol ligands, various coating layers, and Au NPs. In this regard, there is still a lack of sufficient theoretical researches to thoroughly understand these intricate and energetic interaction processes. Therefore, the systematic and extensive studies are required to move beyond phenomenological observations of LDI-TOF-MS analysis and then clearly understand the detailed LDI processes.

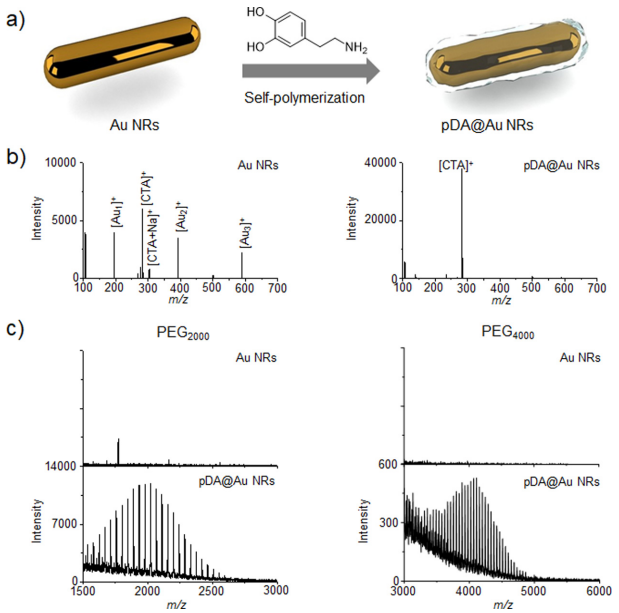

Figure 10. (a) Schematic diagram for the synthesis of pDA@Au NRs. (b) LDI-TOF-MS spectra of Au NRs and pDA@Au NRs. (c) LDI-TOF-MS spectra of PEG_{2000} and PEG_{4000} obtained with Au NRs and pDA@Au NRs, respectively. Reproduced and reprinted with permission from Kang et al. (2017). Copyright 2017 the Royal Society of Chemistry.

Fabrication of Au NS thin films for efficient LDI-TOF-MS analysis

The uniform mass signal is the most important feature in Au NSs-assisted LDI-TOF-MS analysis of small molecules because it is directly related to applicability for quantitative analysis.[34] However, it is still difficult to achieve homogeneous mass signals with colloidal Au NPs because the "coffee-ring effect" generally occurs when the Au NPs are dried with analytes on a target plate under ambient condition for LDI-TOF-MS analysis.[35] Therefore, there were many efforts to solve the critical problem of uneven mass signals which originates from the inhomogeneous distribution of Au NPs.[36] The surface immobilization of colloidal Au NPs on a solid substrate is a promising approach considering that the Au NPs can be immobilized on solid substrates with a high surface coverage through various chemical interactions,[37] and the surface immobilized Au NPs are free from the uncontrolled aggregation in a colloidal state. It is worthy to note that the structural parameters such as thickness, porosity, and surface area can be controlled with the well-established colloidal and surface chemistry of Au NPs and solid substrates. For example, the thickness, porosity, and surface area of the surface immobilized Au NPs can be finely tuned with layer-by-layer (LBL) assembly process of Au NPs and polyelectrolytes based on their strong electrostatic interaction.[38]

Arakawa et al. showed that the LBL assembly of citrate-stabilized Au NPs presenting negatively charges and polyallylamine hydrochloride (PAAH) presenting positively charges.[39] The successive LBL assembly of Au NPs and

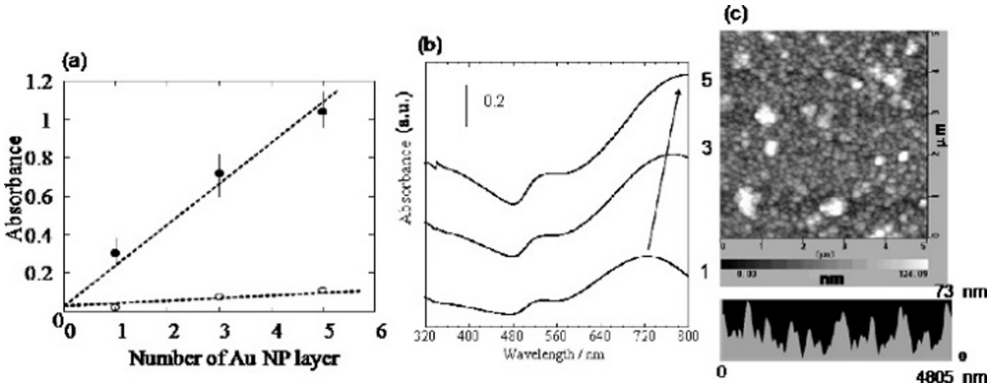

Figure 11. (a) The absorbance at 337 nm and (b) overall absorption spectra of LBL assembled thin films of Au NPs on quartz substrates. (c) AFM images of LBL assembled thin films of Au NPs. Reprinted with permission from Kawasaki et al. (2008). Copyright 2008 American Chemical Society.

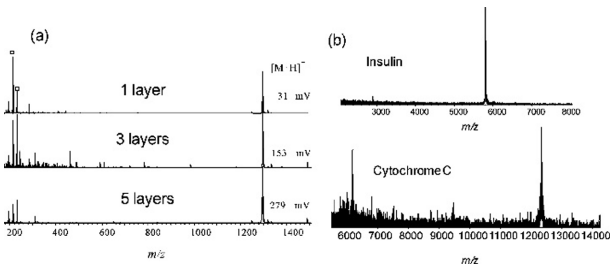

Figure 12. (a) LDI-TOF-MS spectra of angiotensin I obtained on the 1, 3, and 5 cycle LBL assembled thin films of Au NPs. The intensities of mass peaks are indicated in millivolt in the figure. (b) LDI-TOF-MS spectra of insulin and cytochrome c obtained from the 5 LBL assembled thin films of Au NPs. Reprinted with permission from Kawasaki et al. (2008). Copyright 2008 American Chemical Society.

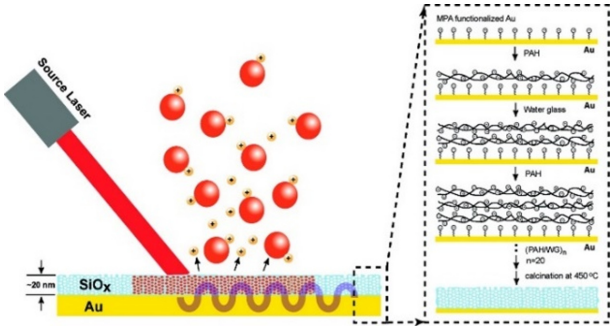

Figure 13. Schematic diagram of LDI-TOF-MS analysis on the silica@Au thin films. Reprinted with permission from Duan et al. (2010). Copyright 2010 American Chemical Society.

PAAH was confirmed by monitoring the linear and continuous increase of the absorbance at 337 nm which is matched with the laser wavelength equipped in LDI-TOF-MS (Figure 11a). The optical absorption of LBL assembled Au NPs increased with the number of LBL assembly cycles throughout the overall UV-Vis region (Figure 11b). The optimum LBL assembly cycle of Au NPs and PAAH was determined to be 5, and the resulting 5 LBL assembled thin film of Au NPs has a highly-compacted structures with numerous nanogaps (Figure 11c).

The LDI-TOF-MS analysis of angiotensin I (1,296.5 Da) was much more efficient on 5 LBL assembled thin films of Au NPs than 1 and 3 LBL assembled thin films of Au NPs (Figure 12a). The analytes with higher molecular weight such as insulin (5.8 kDa) and cytochrome c (12.4 kDa) were also successfully detected on the 5 LBL assembled thin films of Au NPs (Figure 12b). The high efficiency in LDI-TOF-MS analysis of large biomolecules indicated that the LBL assembled Au NPs are a promising platform, and there was no significant variation of mass signal intensities at the different positions.[39] This high and homogeneous LDI efficiency of 5 LBL assembled Au thin films was

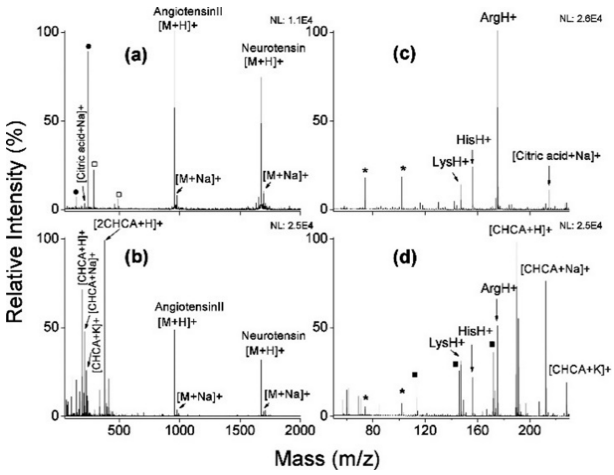

Figure 14. LDI-TOF-MS spectra of (a) angiotensin II and neurotensin mixtures obtained on silica@Au thin film and (b) with CHCA organic matrix. LDI-TOF-MS spectra of Lys, His, and Arg mixture obtained on (c) silica@Au thin films and (d) with CHCA organic matrix. Reprinted with permission from Duan et al. (2010). Copyright 2010 American Chemical Society.

attributed to the increased UV laser absorption, decreased thermal conductivity owing to presence of PAAH in the LBL assembled films, increase of the surface roughness (~100 nm), and uniform LBL assembled structure.[39] This study showed that a strong potential of the nanohybrid thin films composed of Au NPs and various coating layers with a low thermal conductivity for the efficient LDI-TOF-MS analysis of small and large molecules.

Duan et al. developed a strategy to construct a novel nanohybrid films composed Au nanofilm and silica thin coating layer as an optically-active component for LDI-TOF-MS analysis and thermally insulating component for local heat confinement, respectively.[40] Au nanofilm was prepared on a glass substrate with an adhesive Cr layer by e-beam deposition. The Au nanofilms were functionalized with 3-mercaptopropanoic acid (3-MPA) to introduce carboxylic acid groups presenting a negative charge, and the 3-MPA functionalized Au nanofilms were coated with silicate layers through LBL assembly cycles of PAAH and sodium silicate as negative and positive polyelectrolytes, respectively (Figure 13). The resulting Au nanofilms coated with LBL assembled layers of sodium silicate and PAAH were calcinated at 450°C under air atmosphere to convert the LBL assembled layers into silica thin films (Figure 13). The low thermal conductivity of silica thin films makes the Au nanofilms suitable for LDI-TOF-MS analysis by preventing the rapid dissipation of locally-generated thermal energy by laser irradiation during LDI-TOF-MS analysis.

The calcinated silica coated Au (silica@Au) nanofilms were applied to LDI-TOF-MS analysis of two peptides ([Sar1, Thr8]-angiotensin II (956.1 Da) and neurotensin (1,672 Da)) and three amino acids (Lys, His, and Arg). The

petides were successfully detected on the silica@Au nanofilms as a protonated adducts $[M+H]^+$ with a clear background signal whereas MALDI-TOF-MS spectrum of the equal peptide mixture presented strong noise peaks derived from the adducts of CHCA matrix (Figure 14a, b). The amino acid mixture of Lys, His, and Arg was also clearly detected on the silica@Au nanofilms, and there were also clear and strong mass peaks corresponding to their protonated adducts $[M+H]^+$ with a clear background signal (Figure 14c). The amino acid mixture was also analyzed by using CHCA matrix, but in that case, there were many strong noise peaks derived from the fragmentation and adduct formation of CHCA (Figure 14d). In addition to the peptides, small proteins such as insulin chain b (3.5 kDa) and cytochrome c (12.4 kDa) were also detected on the silica@Au nanofilms with a clear background signal, and the LDI efficiency of peptides and proteins on the silica@Au nanofilms was further enhanced with addition of citric acid as a proton donor. Those results clearly demonstrated that the silica@Au thin films can be utilized as a LDI-TOF-MS analysis platform for various analytes.

The silica@Au nanofilms were further improved for efficient LDI-TOF-MS analysis by using the surface immobilized Au NPs as an optically-active component instead of the e-beam deposited Au nanofilms.[41] The monolayered Au NPs was fabricated on a glass substrate through the piranha treatment followed by adsorption of PAAH, and the monolayer of citrate-stabilized Au NPs was coated with an ultra silica layer by single LBL assembly cycle of PAAH and sodium silicate followed by the calcination process at 450°C under air atmosphere. This process lead to formation of the silica@Au NP films composed of the densely-packed Au NPs with nanoscale silica coating layer (2 nm) with numerous nanogaps. Owing to this interesting structure, the thermal energy is efficiently generated by laser irradiation and then locally confined at the laser-irradiated region during LDI-TOF-MS analysis. The theoretical finite-difference time-domain (FDTD) simulation confirmed that the silica@Au NP films have a totally different physicochemical properties with the Au nanofilms prepared by e-beam deposition. These silica@Au NP films also resulted in a highly efficient LDI-TOF-MS analysis of peptides such as [Sar1, Thr8]-angiotensin II (956.1 Da), neurotensin (1,672 Da), and trypsin digest of cytochrome c with a clear background signal and without generation of the undesired Au cluster ions.

Those reports exhibited that the surface immobilized Au NPs can be an efficient platform for LDI-TOF-MS analysis with a homogeneous mass signal, and their LDI-TOF-MS efficiency was further enhanced by coating with a thermally insulating layer. However, the nanohybrid structure of Au NPs can be varied with diverse materials having a different function with thermally insulating silica. Kim et al. demonstrated that Au NPs can be immobilized on the functionalized graphene oxide (GO) thin film with PAAH and further grown through the seed-mediated growth for enhancement of laser energy absorption capacity (Figure 15a).[42] The Au

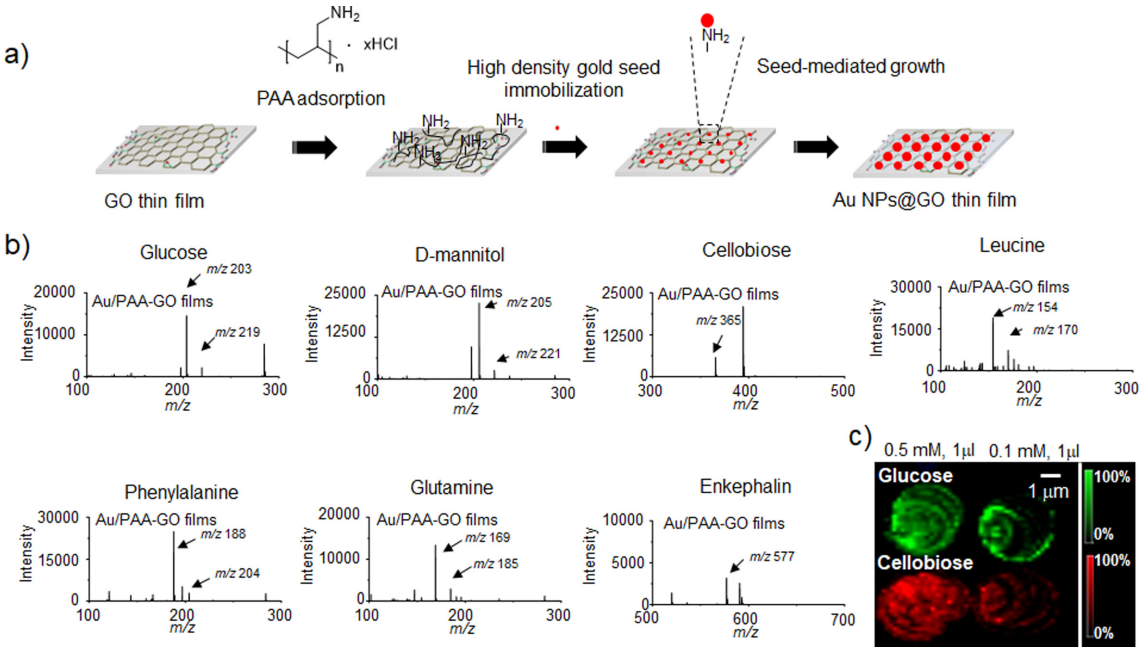

Figure 15. (a) Schematic diagram of preparation process for the Au NPs@GO thin films. (b) LDI-TOF-MS spectra of glucose, mannitol, cellobiose, Leu, Phe, Glu, and Leu-enkephalin obtained from Au NPs@GO thin films. (c) LDI-TOF-MS image of glucose and cellobiose obtained from Au NPs@GO thin films. Reproduced and reprinted with permission from Kim et al. (2012). Copyright 2012 American Chemical Society.

NPs grown GO (Au NPs@GO) thin films were successfully applied to LDI-TOF-MS analysis of small molecules such as glucose, mannitol, cellobiose, Leu, Phe, Glu, and Leu-enkephalin with a clear background signal (Figure 15b). The LDI efficiency of Au NPs@GO thin films was much higher than that of Au NPs and GO thin films alone. The high LDI efficiency of Au NPs@GO thin films was ascribed to the synergistic effect between Au NPs and GO as optically-active components for the laser absorption and improved thermal conductivity for the rapid heat dissipation to prevent excess heating.[42] LDI-TOF-MS imaging of glucose and cellobiose with different concentrations verified that the mass signals from the Au NPs@GO thin films was homogeneous and concentration dependent for quantitative analysis (Figure 15c).[42]

Self-Assembled arrays of Au NPs at liquid-liquid interfaces for LDI-TOF-MS analysis of small molecules

As described in the former subsection, fabrication of the uniform Au NSs on a substrate is of the utmost importance to develop an uniform LDI-TOF-MS platform for quantitative analysis of small molecules. Recently, the self-assembly of Au NPs at liquid-liquid interfaces has attracted much research interest owing to its simplicity, cost-effectiveness, and ability to induce formation of the ordered and compact arrays.[43] Wang et al. demonstrated an interfacial self-assembly of the oppositely charged Au NPs with the decreased interfacial energy.[44] The as-synthesized Au NPs have a negatively charged surface owing to the surface-adsorbed citrates, and Cyst-Au NPs have a positively charged surface. The citrate-stabilized Au NPs were mixed with dichloroethane (DCE) to form oil-water interface, and then the Cyst-Au NPs were added to the mixture. This process lead the interfacial assembly of the oppositely charged Au NPs together with sub 3 nm interparticle gaps, and the self-assembled arrays were sequentially transferred on the Si substrate by using micropipette (Figure 16a). The transferred arrays of Au NPs were directly utilized as a LDI-TOF-MS platform for quantitative analysis of various metabolites in cerebrospinal fluid (CSF) (Figure 16b).

For example, glucose was successfully detected from the self-assembled arrays of Au NPs prepared on Si substrates with a clear background signal (Figure 17a, b) whereas a pristine Si substrate and smooth Au nanofilm showed no noticeable mass signal of glucose under the equal condition (Figure 17c, d). The mass signal intensity of glucose on the self-assembled arrays of Au NPs was homogeneous, and thus the relative standard deviation (RSD) was only 2.9% when LDI-TOF-MS analysis was carried out on four different positions (Figure 17e). The RSD of glucose mass signal was also 4.8% on six diffferent batches of the self-assembled arrays of Au NPs (Figure 17f). LDI-TOF-MS imaging of glucose on the self-assembled arrays of Au NPs also generated a homogeneous mass signal (Figure 17g, top), but there were only several sweet-spots on the

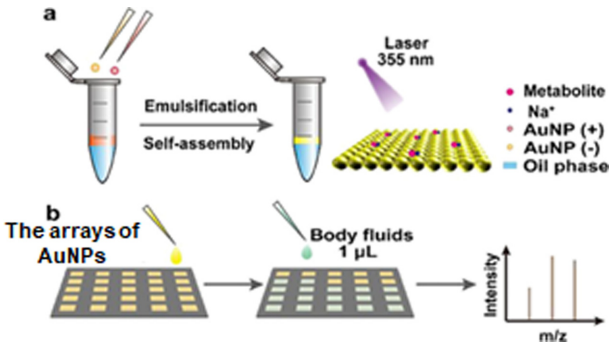

Figure 16. (a) The schematic diagram of the self-assembly of Au NPs at oil-water interface for formation of the compacted arrays and (b) LDI-TOF-MS analysis of CSF on the arrays of Au NPs. Reproduced and reprinted with permission from Wang et al. (2021). Copyright 2021 American Chemical Society.

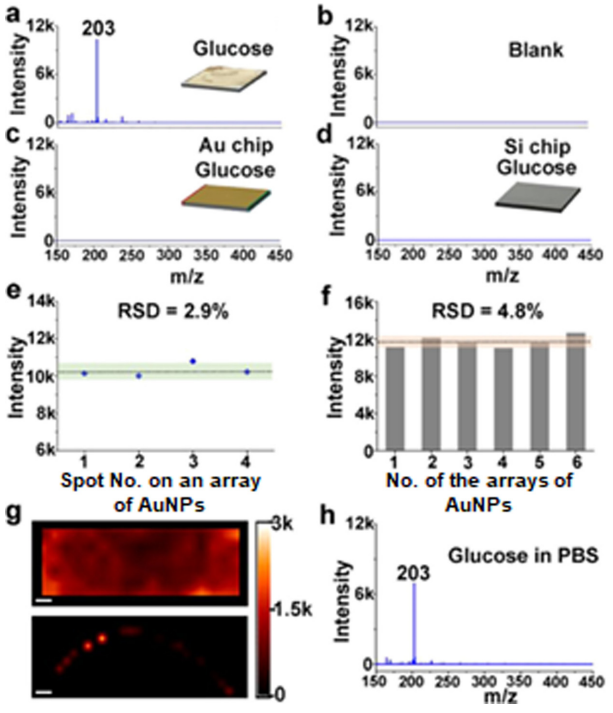

Figure 17. LDI-TOF-MS spectra of (a) glucose and (b) blank samples obtained on the self-assembled arrays of Au NPs. LDI-TOF-MS spectra on glucose obtained on (c) a smooth Au thin films fabricated by sputtering process and (d) a native Si substrate. Mass signal intensities of glucose at (e) four different positions and (f) six different arrays. g) LDI-TOF-MS imaging results of glucose using (top) the self-assembled arrays and (bottom) aggregates of Au NPs of glucose. h) LDI-TOF-MS spectrum of glucose in 1 mM PBS obtained on self-assembled arrays of Au NPs. Reproduced and reprinted with permission from Wang et al. (2021). Copyright 2021 American Chemical Society.

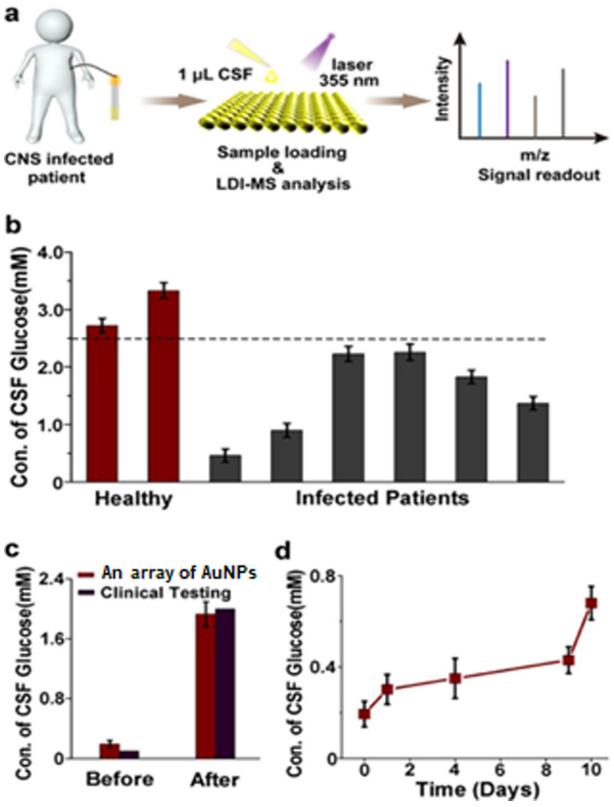

Figure 18. (a) Schematic diagram of CSF analysis on the self-assembled arrays of Au NPs. (b) Concentration of glucose in CSF of the patients and healthy controls obtained by LDI-TOF-MS analysis using the self-assembled arrays of Au NPs. Glucose concentrations of (c) a patient before and after treatment and (d) the patient with treatments for 10 days obtained LDI-TOF-MS analysis on the self-assembled arrays of Au NPs. Reproduced and reprinted with permission from Wang et al. (2021). Copyright 2021 American Chemical Society.

aggregated Au NPs (Figure 17g, bottom). In addition, the self-assembled arrays of Au NPs were applied to LDI-TOF-MS analysis of glucose dissolved in phosphate buffered saline (PBS). Although the mass signal of glucose decreased slightly, it was still clearly detected on the self-assembled arrays of Au NPs (Figure 17h). Those results indicated that the self-assembly strategy is promising to fabricate the uniform self-assembled arrays of Au NPs which can provide a homogeneous mass signal for quantitative analysis of metabolites.

The self-assembled arrays of Au NPs were then applied to quantitative LDI-TOF-MS analysis of glucose level in CSF from a child suffering from the severe intracranial infection for evaluating the treatment efficacy and guiding clinical treatment. The quantitative LDI-TOF-MS analysis results were consistent with that the results of enzyme-based clinical biochemical assay, which is harnessed as a standard method for monitoring glucose level in CSF. The detection time was considerably shortened with LDI-TOF-MS analysis on the arrays of Au NPs from 30 to 5 min. This simple, rapid, and quantitative analysis is of the most important feature of LDI-TOF-MS analysis for the clinical diagnosis and therapeutic monitoring applications .

Based on the advantages of the interfacial self-assembly, an interesting self-assembly strategy was developed by using b-cyclodextrin (b-CD) functionalized Au (b-CD-Au) NPs for LDI-TOF-MS analysis.[45] b-CD has hydrophobic pocket, and thus b-CD-Au NPs can be self-assembled with tetrakis (4-carboxyphenyl) porphyrin (TCPP) as a spacer at the DCE/water interface. The self-assembled arrays of b-CD-Au NPs has regular interparticle gaps which act as hot spots for electromagnetic (EM) field enhancement.[46] The arrays of b-CD-Au NPs were directly applied to LDI-TOF-MS analysis of metabolites in CSF. Various metabolites were detected on the arrays of b-CD-Au NPs with small RSD values of 8.3% and 4.3% for four different positions on a single array and five random spots among different arrays, respectively. The results showed that the host-guest chemistry assisted self-assembly lead to formation of the uniform arrays of Au NPs for a reproducible LDI-TOF-MS analysis. The quantitative analysis was also achieved by using Trp as an internal standard with a linear relationship ($R^2 = 0.992$), and then this LDI-TOF-MS platform was applied to clinical CSF assay for diagnosis of medulloblastoma. LDI-TOF-MS analysis was carried out on the arrays of b-CD-Au NPs with 15 CSF samples to find the difference in molecular patterns of medulloblastoma patients (n = 11) and non-tumor controls (n = 4). Original LDI-TOF-MS spectra of 15 CSF samples at a *m/z* range of 100 – 600 were obtained, and the information of mass peaks were extracted for principal component analysis (PCA) of the *m/z* features.[47] This process clearly discriminated the medulloblastoma patients from the non-tumor controls by using the results of LDI-TOF-MS analysis.

The interfacial self-assembly strategy was further extended to hyperbranched Au (HybrAu) NPs to construct their self-assembled arrays for LDI-TOF-MS based diagnosis of renal cell carcinoma (RCC) with an improved sensitivity (Figure 19).[48] HybrAu NPs were harnessed owing to their sharp tips which considerably enhance EM field.[49] The HybrAu NPs were mixed with Cyst-Au NPs and self-assembled together at the DCE/water interface. The arrays of HybrAu NPs were successfully applied to LDI-TOF-MS analysis with a higher performance than spherical Au NPs owing to the synergy of their sharp tips[49] and nanoscale interparticle gaps which act as hot-spots for EM field enhancement.[46] The enhanced EM and temperature fields were confirmed with theoretical simulation by using spherical Au and HybrAu NPs.[50] HybrAu NPs lead to 4.5-fold higher EM field enhancement than spherical Au NPs, and the EM field of HybrAu NPs was further enhanced with the closely-packed structures formed by the interfacial self-assembly process (Figure 20a). Likewise, the surface tem-

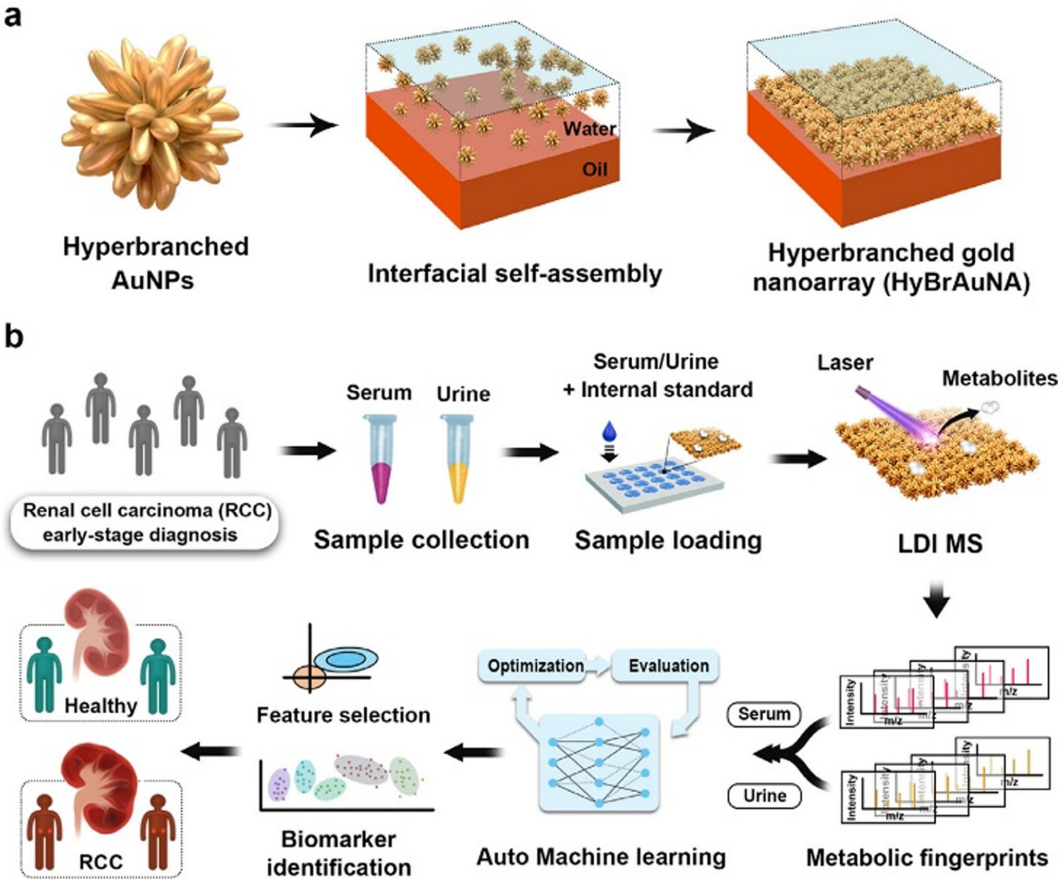

Figure 19. (a) Schematic diagram for preparation of the self-assembled arrays of HybrAu NPs and (b) LDI-TOF-MS analysis based on the arrays of HybrAu NPs to extract SMF, UMF, and S-UMF and then conduct the automated machine learning process to distinguish early-stage RCC patients from healthy controls. Reprinted with permission from Wang et al. (2024). Copyright 2024 American Chemical Society.

perature was also simulated to be higher on the HybrAu NPs (366 K) than the spherical Au NPs (327 K) under the equal simulation condition (Figure 20b). Those results showed that the theoretical simulation is useful to understand the detailed LDI mechanism.

Model metabolites dissolved in complex media were successfully detected on the arrays of HybrAu NPs without interference from salts and proteins while several mass signals of metabolites were compromised with spherical Au NPs under the equal condition (Figure 20c). A shot-to-shot repeatability of mass signal intensity was also verified on the arrays of HybrAu NPs with small RSD values (~5%) (Figure 20d). The limit of detection of glucose was 10 pmol, and the dynamic range was from 10 mM to 1 mM with a linear relationship (R^2 = 0.999) (Figure 20e). The reproducibility of mass signal on the arrays of HybrAu NPs was also confirmed with five different batches (RSD value = 1.3%) (Figure 20f). Then, the arrays of HybrAu NPs were applied to profiling metabolic variation of serum and urine collected from RCC patients (n = 47) and healthy controls (n = 50) for RCC diagnosis. The original LDI-TOF-MS spectra of metabolites were obtained at a *m/z* range of 100 – 600, and the information of mass peaks at m/z 369 and 141 was extracted from the raw data as serum metabolite fingerprint (SMF), urine metabolite fingerprint (UMF), and united SMF and UMF (S-UMF) for PCA to discriminate RCC patients from healthy controls.

However, the speration was not clear between RCC patients and healthy controls, and thus an advanced machine learning was conducted to further improve discrimination.[51] AutoML, an emerging machine learning technology, was utilized to built classification models to achieve optimum classifier algorithms and fine-tuned hyperparameters.[52] After comparing different RCC early stage diagnosis models by AutoML analysis of SMF, UMF, and S-UMF databases, the discrimination performance of RCC patients from healthy controls was greatly improved in comparison with unsupervised analysis. As expected, the discrimination performance was higher with S-UMF database than SMF and UMF databases obtained from the LDI-

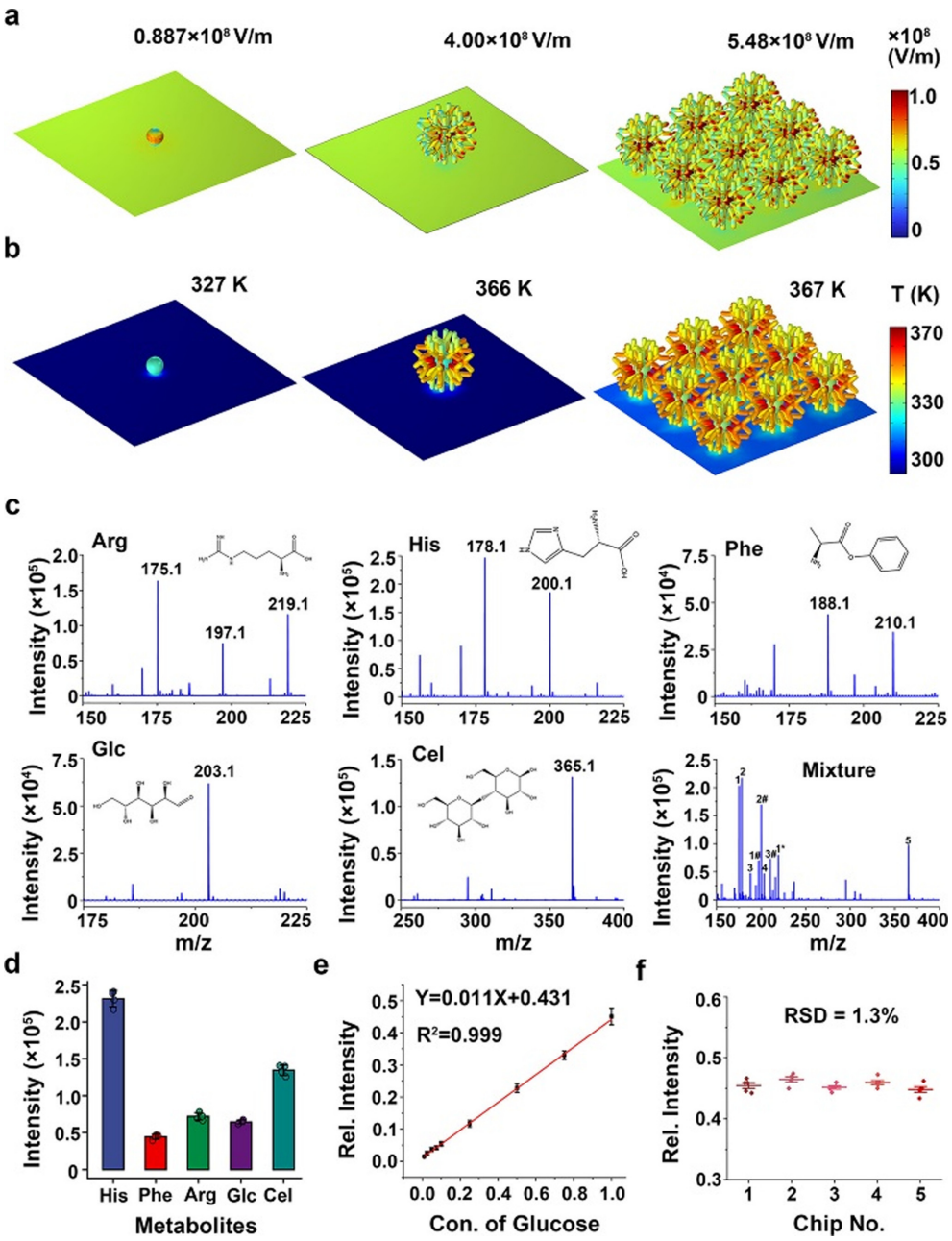

Figure 20. (a) EM field and (b) temperature simulation of the self-assembled arrays of HybrAu NPs. (c) LDI-TOF-MS spectra of Arg, His, Phe, glucose, cellobiose, and their mixture. (d) The mass signal intensities and shot-to-shot repeatability of individual metabolites obtained from different positions on the single array of HybrAu NPs. (e) Quantitative LDI-TOF-MS analysis of glucose using cellobiose as an internal standard. (f) Mass signal reproducibility of five different arrays of HybrAu NPs with an internal standard. Reprinted with permission from Wang et al. (2024). Copyright 2024 American Chemical Society.

TOF-MS analysis of clinical samples on the arrays of HybrAu NPs. Those studies showed the progress of LDI-TOF-MS technique in clinical diagnosis from the simple quantitative analysis to statistical data science with an advanced machine learning.

Conclusions

This review covers a wide variety of Au NSs, including the changes in the physicochemical properties based on their morphology, surface characteristics, composition, and self-assembled structures, for their successful application in

LDI-TOF-MS analysis. Previous reports mainly focus on changes in the LDI efficiency of Au NSs according to their physicochemical properties to enhance the analytical performance for LDI-TOF-MS analysis. The significant strategies to improve LDI-TOF-MS analysis using Au NSs are categorized into morphology control, surface functionalization, surface immobilization, and self-assembly at the oil-water interface. This is not only intriguing for fundamental researches on the correlation between the structure and properties of Au NSs but also holds the potential for developing an effective LDI-TOF-MS platform applicable across a wide range of molecular weights. With high specificity and sensitivity from the previously developed analysis techniques, LDI-TOF-MS using Au NSs attracts more interests from analytical chemists, biologists, physicians, and pharmaceutical engineers. Through a close collaboration of those researchers, the extensive data from LDI-TOF-MS analyses can be acquired, and those data will lead to technological evolution of LDI-TOF-MS analysis by integrating digital data processing technology based on artificial intelligence, finally resulting in a powerful mass spectrometric analysis technique.

Conflict of interest

There are no conflicts to declare.

Acknowledgments

This work was supported by the Basic Science Research Program through the National Research Foundation of Korea (NRF) funded by the Ministry of Science and ICT (MSIT) (No. 2022R1C1C1008388 and 2009-0082580). This research was also supported by Basic Science Research Program through the National Research Foundation of Korea (NRF) funded by the Ministry of Education (2022R1A6A1A03053343).

References

1. Karas, M.; Bachman, D.; Bahr, U.; Hillenkamp, F. *Int. J. Mass Spectrom. Ion Process* **1987**, *78*, 53–68. https://doi.org/10.1016/0168-1176(87)87041-6.
2. Comon, B.; Aebersold, R.; *Science* **2006**, *312*, 212–217. https://doi.org/10.1126/science.1124619.
3. Rainer, M.; Qureshi, M.N.; Bonn, G. K.; *Anal. Bioanal. Chem.* **2011**, *400*, 2281-2288. https://doi.org/10.1007/s00216-010-4138-1.
4. Qiao, Z.; Lissel, F. *Chem. Asian. J.* **2021**, *16*, 868-878. https://doi.org/10.1002/asia.202100044.
5. Peterson, D.S. *Mass Spectrom. Rev.* **2007**, *26*, https://doi.org/10.1002/mas.20104.
6. Tanaka, K.; Waki, H.; Ido, Y.; Akita, S.; Yoshida, Y.; Yoshida, T. *Rapid Commun. Mass Spectrom.* **1988**, *2*, 151-153. https://doi.org/10.1002/rcm.1290020802.
7. Wei, J.; Buriak, J.M.; Siuzdak, G. *Nature* **1999**, *399*, 243–246. https://doi.org/10.1038/20400
8. He, H.; Guo, Z.; Wen, Y.; Xu, S.; Liu, Z. *Anal. Chim. Acta* **2019**, *1090*, 1-22. https://doi.org/10.1016/j.aca.2019.08.048.
9. Guinan, T.; Kirkbride, P.; Paul, E.P.; Ronci, M.; Kobus, H.; Voelcker, N.H. *Mass Spectrom. Rev.* **2015**, *34*, 627-640. https://doi.org/10.1002/mas.21431.
10. Yang, S.S.; Shi, M.Y.; Tao, Z.R.; Wang, C.; Gu, Z.Y. *Anal. Bioanal. Chem.* **2019**, *411*, 4509-4522. https://doi.org/10.1007/s00216-019-01876-1.
11. Kim, Y.-K.; Wang, L.S.; Landis, R.; Kim, C.S.; Vachet, R.W.; Rotello, V.M. *Nanoscale* **2017**, *9*, 10854-10860. https://doi.org/10.1039/c7nr02949g.
12. Kailasa, S.K.; Cheng, K.H.; Wu, H.F. *Materials* **2013**, *6*, 5763-5795. https://doi.org/10.3390/ma6125763.
13. Chae, A.; Jang, H.; Koh, D.Y.; Yang, C.M.; Kim, Y.-K. *Talanta* **2020**, *209*, 120531. https://doi.org/10.1016/j.talanta.2019.120531.
14. Pilolli, R.; Palmisano, F.; Cioffi, N. *Anal. Bioanal. Chem.* **2012**, *402*, 601-623. https://doi.org/10.1007/s00216-011-5120-2.
15. Kim, S.-W.; Kwon, S.; Kim, Y.-K. *Nanomaterials* **2021**, *11*, 288. https://doi.org/10.3390/nano11020288.
16. Abdelhamid, H.N.; Wu, H.F. *Anal. Bioanal. Chem.* **2016**, *408*, 4485-4502. https://doi.org/10.1007/s00216-016-9374-6.
17. Lai, S.K.; Cheng, Y.H.; Tang, H.W.; Ng, K.M. *Phys. Chem. Chem. Phys*. **2017**, *19*, 20795-20807. https://doi.org/10.1039/c7cp04033d.
18. Gámez, F.; Hurtado, P.; Castillo, P.M.; Caro, C.; Hortal, A.R.; Zaderenko, P.; Martínez–Haya, B. *Plasmonics* **2010**, *5*, 125-133. https://doi.org/10.1007/s11468-010-9125-z.
19. Castellana, E.T.; Russell, D.H. *Nano Lett.* **2007**, *7*, 3023-3025. https://doi.org/10.1021/nl071469w.
20. Kawasaki, H.; Sugitani, T.; Watanabe, T.; Yonezawa, T.; Moriwaki, H.; Arakawa, R. *Anal. Chem.* **2008**, *80*, 7524-7533. https://doi.org/10.1021/ac800789t.
21. Wang, Y.; Zhang, K.; Tian, T.; Shan, W.; Qiao, L.; Liu, B. *ACS Appl. Mater. Interfaces.* **2021**, *13*, 4886-4893. https://doi.org/10.1021/acsami.0c20944.
22. Bansal, S.A.; Kumar, V.; Karimi, J.; Singh, A.P.; Kumar, S. *Nanoscale Adv.* **2020**, *2*, 3764-3787. https://doi.org/10.1039/d0na00472c.
23. McLean, J.A.; Stumpo, K.A.; Russell, D.H. *J. Am. Chem. Soc.* **2005**, *127*, 5304-5035. https://doi.org/10.1021/ja043907w.
24. Castellana, E.T.; Gamez, R.C.; Gómez, M.E.; Russell, D.H. *Langmuir* **2010**, *26*, 6066-6070. https://doi.org/10.1021/la904467b.
25. Mout, R.; Moyano, D.F.; Rana, S.; Rotello, V.M. *Chem. Soc. Rev.* **2012**, 41, 2539-2544. https://doi.org/10.1039/c2cs15294k.
26. Vericat, C.; Vela, M.E.; Salvarezza, R.C. *Phys. Chem. Chem. Phys.* **2005**, *7*, 3258-3268. https://doi.org/10.1039/b505903h.

27. Bajaj, M.; Wangoo, N.; Jain, D.V.S.; Sharma, R.K. *Sci. Rep.* **2020**, *10*, 8213. https://doi.org/10.1038/s41598-020-65013-0.
28. Duan, J.; Linman, M.J.; Chen, C.-Y.; Cheng, Q. *J. Am. Soc. Mass Spectrom.* **2009**, *20*, 1530-1539. https://doi.org/10.1016/j.jasms.2009.04.009.
29. Castellana, E.T.; Russell, D.H. *Nano Lett.* **2007**, *7*, 3023-3025. https://doi.org/10.1021/nl071469w.
30. Palermo, A.; Forsberg, E.M.; Warth, B.; Aisporna, A.E.; Billings, E.; Kuang, E.; Benton, H.P.; Berry, D.; Siuzdak, G. *ACS Nano* **2018**, *12*, 6938-6948. https://doi.org/10.1021/acsnano.8b02376.
31. Kurczy, M.E.; Zhu. Z.J.; Ivanisevic. J.; Schuyler. A.M.; Lalwani. K.; Santidrian, A.F.; David, J.M.; Giddabasappa, A.; Roberts, A.J.; Olivos, H.J.; O'Brien, P.J.; Franco, L.; Fields, M.W.; Paris, L.P.; Friedlander, M.; Johnson, C.H.; Epstein, A.A.; Gendelman, H.E.; Wood, M.R.; Felding, B.H.; Patti, G.J.; Spilker, M.E.; Siuzdak, G. *Nat. Commun*. **2015**, *6*, 5998. https://doi.org/10.1038/ncomms6998.
32. Wu, R.; Li, L.; Deng, C. *Proteomics* **2016**, *16*, 1311-1320. https://doi.org/10.1002/pmic.201500383.
33. Kang, K.; Jang, H.; Kim, Y.-K. *Analyt* **2017**, *142*, 2372-2377. https://doi.org/10.1039/c7an00356k.
34. Korte, A.R.; Morris, N.J.; Vertes, A. *Anal. Chem.* **2019**, *91*, 3951-3958. https://doi.org/10.1021/acs.analchem.8b05074.
35. Yukird, J.; Kaminsky, C.J.; Chailapakul, O.; Rodthongkum, N.; Vachet, R.W. *J. Am. Soc. Mass Spectrom.* **2021**, *32*, 1780-1788. https://doi.org/10.1021/jasms.1c00132.
36. Hansen, R.L.; Dueñas, M.E.; Lee, Y.J. *J. Am. Soc. Mass Spectrom.* **2019**, *30*, 299-308. https://doi.org/10.1007/s13361-018-2081-0.
37. Thomas, N.; Sreekeerthi, P.; Swaminathan, P. *Phys. Chem. Chem. Phys.* **2022**, *24*, 25025-25035. https://doi.org/10.1039/d2cp01004f.
38. Chen, Y.F.; Lee, Y.C.; Lin, W.W.; Lu, M.C.; Yang, Y.C.; Chiu, C.W. *ACS Omega,* **2023**, *9*, 1894-1903. https://doi.org/10.1021/acsomega.3c08608.
39. Kawasaki, H.; Sugitani, T.; Watanabe, T.; Yonezawa, T.; Moriwaki, H.; Arakawa, R. *Anal Chem.* **2008**, *80*, 7524-7533. https://doi.org/10.1021/ac800789t.
40. Duan, J.; Linman, M.J.; Cheng, Q. *Anal. Chem.* **2010**, *82*, 5088–5094. https://doi.org/10.1021/ac100132x.
41. Chen, C.-Y.; Hinman, S.S.; Duan, J.; Cheng, Q. *Anal. Chem.* **2014**, *86*, 11942−11945. https://doi.org/10.1021/ac503808r.
42. Kim, Y.-K.; Min, D.-H. *Langmuir* **2012**, *28*, 4453−4458. https://doi.org/10.1021/la204185p.
43. Li, J.; Wang, Q.; Wang, J.; Li, M.; Zhang, X.; Luan, L.; Li, P.; Xu, W. *Anal. Bioanal. Chem.* **2021**, *413*, 4207-4215. https://doi.org/10.1007/s00216-021-03366-9.
44. Wang, Y.; Zhang, K.; Tian, T.; Shan, W.; Qiao, L.; Liu, B. *ACS Appl. MACHINE LEARNING, AUTOML, mass spectrometryMater. Interfaces* **2021**, *13*, 4886−4893. https://doi.org/10.1021/acsami.0c20944
45. Wang, Y.; Liu, Y.; Yang, S.; Yi, J.; Xu, X.; Zhang, K.; Liu, B.; Qian, K. *Small* **2023**, *19*, 2207190. https://doi.org/10.1002/smll.202207190.
46. Lee, J.H.; Oh, J.W.; Nam, S.H.; Cha, Y.S.; Kim, G.H.; Rhim, W.K.; Kim, N.H.; Kim, J.; Han, S.W.; Suh, Y.D.; Nam, J.M. *Small* **2016**, *12*, 4726-4734. https://doi.org/10.1002/smll.201600289.
47. Patel, N.; Alkhouri, N.; Eng, K.; Cikach, F.; Mahajan, L.; Yan, C.; Grove, D.; Rome, E.S.; Lopez, R.; Dweik, R.A. *Aliment. Pharmacol. Ther.* **2014**, *40*, 498-507. https://doi.org/10.1111/apt.12861.
48. Wang, Y.; Xu, X.; Fang, Y.; Yang, S.; Wang, Q.; Liu, W.; Zhang, J.; Liang, D.; Zhai, W.; Qian, K. *ACS Nano* **2024**, *18*, 2409-2420. https://doi.org/10.1021/acsnano.3c10717.
49. Liu, H.; Zeng, J.; Song, L.; Zhang, L.; Chen, Z.; Li, J.; Xiao, Z.; Su, F.; Huang, Y. *Nanoscale Horiz.* **2022**, *7*, 554-561. https://doi.org/10.1039/d2nh00023g.
50. Velázquez-Salazar, J.J.; Bazán-Díaz, L.; Zhang, Q.; Mendoza-Cruz, R.; Montaño-Priede, L.; Guisbiers, G.; Large, N.; Link, S.; José-Yacamán, M. *ACS Nano*, **2019**, *13*, 10113-10128. https://doi.org/10.1021/acsnano.9b03084.
51. Yuan, B.; Lyu, W.; Dinssa, F.F.; Simon, J.E.; Wu, Q. *J. Chromatogr. A* **2021**, *1637*, 461733. https://doi.org/10.1016/j.chroma.2020.461733.
52. Salehin, I.; Islam, Md.S.; Saha, P.; Noman, S.M.; Tuni, A.; Hasan, Md.M.; Baten, Md.A. *J. Artif. Intell.* **2024**, *2*, 52-81. https://doi.org/10.1016/j.jiixd.2023.10.002